J Eng Math (2009) 64:1–13
DOI 10.1007/s10665-008-9248-9

Mixed convection flow near an axisymmetric stagnation point on a vertical cylinder

Cornelia Revnic · Teodor Grosan · John Merkin · Ioan Pop

Received: 24 January 2008 / Accepted: 16 September 2008 / Published online: 10 October 2008

Abstract The mixed convection flow near an axisymmetric stagnation point on a vertical cylinder is considered. The equations for the fluid flow and temperature fields reduce to similarity form that involves a Reynolds number R and a mixed convection parameter λ, as well as the Prandtl number σ. Numerical solutions are obtained for representative values of these parameters, which show the existence of a critical value $\lambda_c = \lambda_c(R, \sigma)$ for the existence of solutions in the opposing ($\lambda < 0$) case. The variation of λ_c with R is considered. In the aiding ($\lambda > 0$) case solutions are possible for all λ and the asymptotic limit $\lambda \to \infty$ is obtained. The limits of large and small R are also treated and the nature of the solution in the asymptotic limit of large Prandtl number is briefly discussed.

Keywords Asymptotic solutions · Axisymmetric stagnation flow · Boundary layers · Dual solutions · Mixed convection

1 Introduction

Combined forced- and free-convection flows (mixed convection) are encountered in many technological and industrial applications including solar receivers exposed to wind currents, electronic devices cooled by fans, nuclear reactors cooled during emergency shutdown, heat exchanges placed in a low-velocity environment and many more. Two-dimensional stagnation-point flows arise in the vicinity of a stagnation line resulting from a two-dimensional flow impinging on a curved surface at right angles to it and thereafter flowing symmetrically about the stagnation line. Hiemenz [1] was the first to study two-dimensional stagnation-point flows. Later Eckert [2] and Gorla [3] considered the corresponding forced-convection heat-transfer problem. Three-dimensional stagnation-point flows have been studied by Homann [4] and Smith [5] and the axisymmetric stagnation-point flow on a circular cylinder by Wang [6] and Gorla [7]. The three-dimensional flow resulting from an axisymmetric stagnation flow

C. Revnic
Tiberiu Popoviciu Mathematical Institute, P.O. Box 68-1, 400110 Cluj, Romania

T. Grosan · I. Pop
Applied Mathematics, Babes-Bolyai University, CP 253, 3400 Cluj, Romania

J. Merkin (✉)
Department of Applied Mathematics, University of Leeds, Leeds LS2 9JT, UK
e-mail: amtjhm@maths.leeds.ac.uk

impinging obliquely on a body surface has been treated by Weidman and Putkaradze [8]. The problem of axisymmetric stagnation-point flow acting on a porous flat plate oscillating transversely in its own plane has been investigated by Weidman and Mahalingam [9]. In this case a three-dimensional flow results from a stagnation-point flow on a flat plate oscillating in its own plane. Gorla [10] has studied the unsteady viscous flow in the vicinity of an axisymmetric stagnation point on a circular cylinder.

The steady mixed convection flow near the stagnation region of a vertical flat plate has been studied by Ramachandran et al. [11] and by Gorla [12] for the flow near an axisymmetric stagnation point on a slender impermeable vertical cylinder. Mixed convection flows arise when the buoyancy forces resulting from temperature differences within the flow become comparable to the pressure gradient forces arising from the forced flow. As a consequence, both the flow and thermal fields are significantly affected by the buoyancy forces. The study of thick axisymmetric free-convection boundary layers along slender bodies has been shown by Kuiken [13] to have an unusual structure at large distances along the cylinder. When the boundary-layer variables are scaled so as to be of order unity within the boundary layer, the boundary conditions that hold on the surface of the slender body are given at a value of the independent variable which is close to zero. As a result, when a perturbation analysis is used to obtain the solution at large distances along the cylinder, the body is reduced to a line at the first approximation.

Several papers have been published previously on axisymmetric mixed convection boundary-layer flows along slender bodies. Naraian and Uberoi [14,15] and Chen [16] have studied the mixed convection boundary layer on a vertical needle. These are bodies of revolution whose diameter is of the same order as the thickness of the velocity or thermal boundary layers that develop on it. By appropriately varying the radius of the needle, the boundary-layer equations admit similarity solutions. Wang [17] found a similarity solution for the mixed convection boundary layer on an adiabatic vertical needle with a heat source at the tip, a situation that arises, for example, for a stick burning at its lower end.

The present paper considers the steady mixed convection flow that develops near an axisymmetric stagnation point on a vertical isothermal cylinder in the case when the boundary layer is thick compared to the radius of the cylinder. We start by describing the governing equations, following closely [9,12] for the forced-convection problem. This results in two ordinary differential equations for the flow and temperature fields that involve, as well as the Prandtl number σ, the two further parameters R, which is measure of the forced flow, and a mixed convection parameter λ. We consider both aiding flows (when the outer flow and the buoyancy forces are in the same direction, $\lambda > 0$) and opposing flows (when the outer flow and the buoyancy forces act in opposite directions, $\lambda < 0$). We start by giving numerical solutions to these equations for representative values of λ and R, finding dual solutions for negative λ with critical points $\lambda_c < 0$, requiring $\lambda \geq \lambda_c$ for the existence of a solution. We determine how λ_c varies with R, before considering the asymptotic limits of $\lambda \to \infty$ (free-convection limit) and $R \to \infty$ and $R \to 0$.

2 Equations

We consider the steady mixed convection flow near an axisymmetric stagnation point on an infinite cylinder. The cylinder is taken as mounted vertically and the flow is assumed to be axisymmetric about the x-axis, which measures distance along the cylinder in a vertical direction with gravity acting in the negative x-direction. The stagnation point is at $x = 0$, $r = a$, where r measures distance radially from the centre of the cylinder of radius a. The ambient fluid has a constant temperature T_∞ and the cylinder is maintained at a temperature $T_w(x) = T_0\ (x/a) + T_\infty$. Having $T_w > T_\infty$ corresponds to assisting flow, with $T_w < T_\infty$ corresponding to opposing flow. The outer flow in this situation, taken directly from [12], is

$$u = -\left(\frac{U_\infty}{a}\right)\left(r - \frac{a^2}{r}\right), \quad v = 2U_\infty\left(\frac{x}{a}\right), \tag{1}$$

where U_∞ is the planar flow at large distances from the cylinder and where u and v are the velocity components in the x and r directions, respectively.

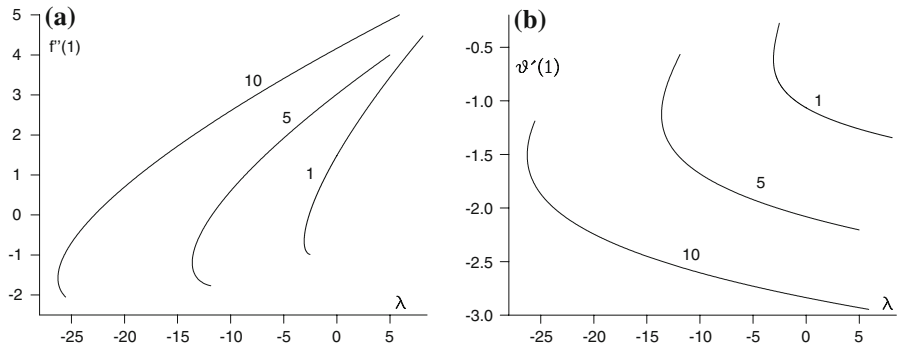

Fig. 1 Plots of (**a**) $f''(1)$ and (**b**) $\theta'(1)$ against λ for $R = 1,\ 5,\ 10$ obtained from the numerical solution of equations (3, 4) subject to boundary conditions (5) for $\sigma = 1$

Again following [12], we introduce the variables

$$\eta = \left(\frac{r}{a}\right)^2, \quad u = -U_\infty \eta^{-1/2} f(\eta), \quad v = 2U_\infty \left(\frac{x}{a}\right) f'(\eta), \quad \theta(\eta) = \frac{T - T_\infty}{T_w - T_\infty}, \tag{2}$$

where T is the temperature of the fluid. Applying (2) in the governing equations and making the standard Boussinesq approximation, we find that our flow is described by the similarity equations, again from [12],

$$\eta f''' + f'' + R(f\, f'' + 1 - f'^2) + \lambda\theta = 0, \tag{3}$$

$$\eta\theta'' + \theta' + \sigma\, R(f\,\theta' - f'\,\theta) = 0, \tag{4}$$

subject to the boundary conditions, from (1), that

$$f(1) = 0,\ f'(1) = 0,\ \theta(1) = 1, \quad f' \to 1,\ \theta \to 0 \quad \text{as} \ \ \eta \to \infty, \tag{5}$$

(primes denote differentiation with respect to η) where σ is the Prandtl number and where

$$R = \frac{U_\infty a}{2\nu}, \quad \lambda = \frac{g\beta a^2 T_0}{8U_\infty \nu} \tag{6}$$

are, respectively, a Reynolds number and a mixed convection parameter, with $\lambda > 0$ corresponding to assisting flow and $\lambda < 0$ corresponding to opposing flow. In (6) ν is the kinematic viscosity of the fluid, g the acceleration due to gravity and β the coefficient of thermal expansion.

The parameters perhaps of most physical interest are the skin friction parameter C_f and the Nusselt number Nu, defined as

$$C_f = \frac{\tau_w}{\rho U_\infty^2}, \quad \text{Nu} = \frac{a q_w}{k(T_w - T_\infty)} \quad \text{where} \ \ \tau_w = \mu \left(\frac{\partial v}{\partial r}\right)_{r=a}, \quad q_w = -k \left(\frac{\partial T}{\partial r}\right)_{r=a}, \tag{7}$$

and where μ and k are the dynamic viscosity and thermal conductivity, respectively. From (2), we have that

$$C_f = 2\left(\frac{x}{a}\right) f''(1), \quad \text{Nu} = -2\theta'(1). \tag{8}$$

The problem given by (3–5) has been considered previously by Gorla [12] who presented a range of numerical results for both aiding and opposing flows. The results given by [12] are only for a specific value of R, namely $R = 100$, with critical points giving a finite range of existence for opposing flows not being identified in [12]. We start by first describing our numerical solutions to Eqs. (3) and (4) subject to boundary conditions (5) for a range of values of λ and R, thus adding to the numerical treatment given by Gorla [12]. Throughout we assume that the Prandtl number σ is of $O(1)$, our numerical results are all for the case when $\sigma = 1$.

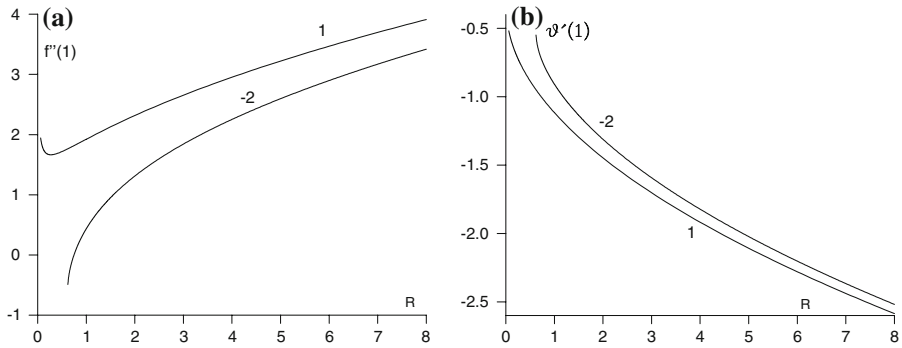

Fig. 2 Plots of (**a**) $f''(1)$ and (**b**) $\theta'(1)$ against R for $\lambda = 1,\ -2$ obtained from the numerical solution of equations (3, 4) subject to boundary conditions (5) for $\sigma = 1$

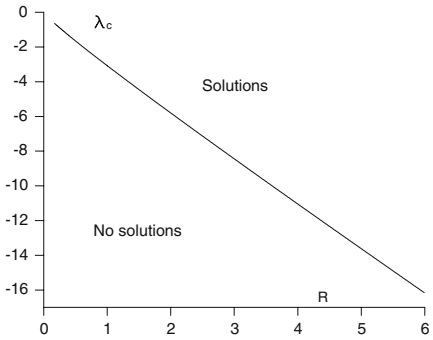

Fig. 3 A plot of the critical value λ_c of λ against R (for $\sigma = 1$). The region in the (λ, R) parameter plane where solutions exist is labelled on the figure

3 Numerical results

Equations (3) and (4) subject to boundary conditions (5) were solved numerically using a standard shooting method for solving boundary-value problems (`D02AGF` in the NAG library). In Fig. 1 we plot $f''(1)$ and $\theta'(1)$ against λ for $R = 1, 5, 10$ (with $\sigma = 1$). This figure shows that, for $\lambda < 0$, there is a critical value λ_c with solutions possible only for $0 > \lambda \geq \lambda_c$ and for $\lambda > \lambda_c$ there are dual solutions. The value of λ_c decreases as R is increased, thus giving a greater range of negative λ for possible solutions. For $\lambda > 0$ there is only one solution with the values of $f''(1)$ increasing and $\theta'(1)$ decreasing as λ is increased (for a given value of R). For the larger values of λ, the values of $f''(1)$ for $R = 1$ becomes greater than those for the larger values of R $(= 5,\ 10)$, indicating that, for sufficiently large values of λ, $f''(1)$ increases as R is decreased. However, the values of $-\theta'(1)$ increase as R is increased (for a given value of λ).

In Fig. 2 we take values for λ $(\lambda = 1,\ -2)$ representative respectively of aiding and opposing mixed convection and plot the corresponding values of $f''(1)$ and $\theta'(1)$ against R. We see that in both cases $\theta'(1)$ decreases as R is increased. However, for $\lambda = 1$, $f''(1)$ has a minimum value, of $f''(1) = 1.6648$ at $R = 0.272$, before increasing again for the larger values of R. For $\lambda = -2$ there is a critical value R_c of R ($R_c \simeq 0.622$) below which there are no solutions, as might be expected from Fig. 1.

3.1 Critical points

We saw in Fig. 1 the existence of a critical value λ_c of λ, requring $\lambda \geq \lambda_c$ for a solution to exist. We can calculate how λ_c varies with R using the appproach described in [18,19]. Essentially we perturb about the solution given by (3, 4) to obtain a linear homogeneous problem. It is then the existence of a nontrivial solution to this homogeneous problem that determines λ_c for a given value of R (and σ). In Fig. 3 we plot λ_c against R, with the figure showing

that λ_c decreases as R is increased, seemingly in a linear manner for the larger values of R, and increases towards zero as R is reduced. The region in the (λ, R) parameter space where solutions exist is labelled on this figure.

Our numerical solutions suggest that considering various limiting forms would give some further insights into the nature of the solution. We now discuss these in more detail, starting with the free-convection limit, $\lambda \to \infty$.

4 Asymptotic results

4.1 λ large

To obtain a solution valid for λ large we start by putting

$$f = \lambda^{1/4} F, \quad \zeta = \lambda^{1/4}(\eta - 1), \tag{9}$$

leaving θ unscaled. This results in the equations

$$(1 + \lambda^{-1/4}\zeta)F''' + \lambda^{-1/4}F'' + R(FF'' - F'^2) + \lambda^{-1}R + \theta = 0, \tag{10}$$

$$(1 + \lambda^{-1/4}\zeta)\theta'' + \lambda^{-1/4}\theta' + \sigma R(F\theta' - F'\theta) = 0, \tag{11}$$

where primes now denote differentiation with respect to ζ, subject to the boundary conditions

$$F(0) = 0,\ F'(0) = 0,\ \theta(0) = 1, \quad F' \to \lambda^{-1/2},\ \theta \to 0 \ \text{ as } \ \zeta \to \infty. \tag{12}$$

Equations (10, 11) suggest looking for a solution by expanding

$$F = F_0 + \lambda^{-1/4}F_1 + \cdots, \quad \theta = \theta_0 + \lambda^{-1/4}\theta_1 + \cdots \tag{13}$$

We can scale the leading-order problem obtained by substituting expansion (13) in (10, 11) by putting

$$F_0 = R^{-3/4}\overline{F}_0, \quad \overline{\zeta} = R^{1/4}\zeta. \tag{14}$$

This results in

$$\overline{F}_0''' + \overline{F}_0\overline{F}_0'' - \overline{F}_0'^2 + \theta_0 = 0, \tag{15}$$

$$\theta_0'' + \sigma(\overline{F}_0\theta_0' - \overline{F}_0'\theta_0) = 0, \tag{16}$$

subject to

$$\overline{F}_0(0) = 0,\ \overline{F}_0'(0) = 0,\ \theta_0(0) = 1, \quad \overline{F}_0' \to 0,\ \theta_0 \to 0 \ \text{ as } \ \overline{\zeta} \to \infty, \tag{17}$$

where primes now denote differentiation with respect to $\overline{\zeta}$. A numerical solution of (15–17) gives, for $\sigma = 1$, $\overline{F}_0''(0) = 0.73950$, $\theta_0'(0) = -0.59509$.

We can continue to the next order by first rescaling

$$F_1 = R^{-1}\overline{F}_1, \quad \theta_1 = R^{-1/4}\overline{\theta}_1. \tag{18}$$

This gives, with (14),

$$\overline{F}_1''' + \overline{F}_0\overline{F}_1'' + \overline{F}_1\overline{F}_0'' - 2\overline{F}_0'\overline{F}_1' + \overline{\theta}_1 = -(\overline{F}_0'' + \overline{\zeta}\,\overline{F}_0'''), \tag{19}$$

$$\overline{\theta}_1'' + \sigma(\overline{F}_0\overline{\theta}_1' + \overline{F}_1\theta_0' - \overline{F}_0'\overline{\theta}_1 - \overline{F}_1'\theta_0) = -(\theta_0' + \overline{\zeta}\,\theta_0''), \tag{20}$$

subject to

$$\overline{F}_1(0) = 0,\ \overline{F}_1'(0) = 0,\ \overline{\theta}_1(0) = 0, \quad \overline{F}_1' \to 0,\ \overline{\theta}_1 \to 0 \ \text{ as } \ \overline{\zeta} \to \infty. \tag{21}$$

A numerical solution gives, again for $\sigma = 1$, that $\overline{F}_1''(0) = 0.06888$, $\overline{\theta}_1'(0) = -0.23452$.

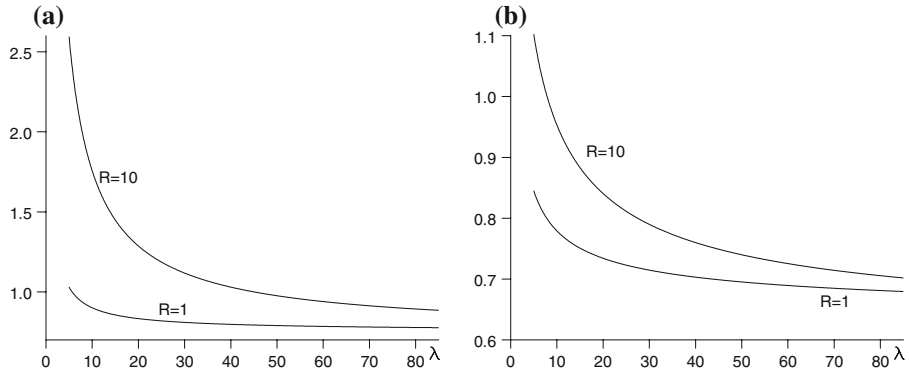

Fig. 4 Plots of $(\lambda^3/R)^{-1/4} f''(1)$ and $-(\lambda R)^{-1/4}\theta'(1)$ obtained from the numerical solution of Eqs. (3, 4) against λ for $R = 1,\ 10$ and $\sigma = 1$

From (9, 14) and (18) we have

$$\left(\frac{\mathrm{d}^2 f}{\mathrm{d}\eta^2}\right)_{\eta=1} \sim \left(\frac{\lambda^3}{R}\right)^{1/4} \left(0.7395 + 0.0689(R\lambda)^{-1/4} + \cdots\right),$$
$$\left(\frac{\mathrm{d}\theta}{\mathrm{d}\eta}\right)_{\eta=1} \sim -(R\lambda)^{1/4} \left(0.5951 + 0.2345(R\lambda)^{-1/4} + \cdots\right) \quad \text{as } \lambda \to \infty. \tag{22}$$

Expressions (22) show that, for sufficiently large values of λ, $-\theta'(1)$ increases as R is increased and that $f''(1)$ decreases as R is increased, in line with Fig. 1. In Fig. 4 we plot the values of $(\lambda^3/R)^{-1/4} f''(1)$ and $-(\lambda R)^{-1/4}\theta'(1)$ obtained from the numerical solution of (3, 4) against λ for $R = 1,\ 10$. In both cases the asymptotic limit for λ large given by (22) is approached as λ increases, though more slowly for $R = 10$ than for $R = 1$ as might be expected from (22).

4.2 R large

To obtain a solution for R large, we follow the approach given in [8] for the forced-convection case and start by writing

$$f = R^{-1/2}\phi, \quad \xi = R^{1/2}(\eta - 1) \tag{23}$$

and leaving θ unscaled. This results in the equations

$$(1 + R^{-1/2}\xi)\phi''' + R^{-1/2}\phi'' + 1 + \phi\phi'' - \phi'^2 + \lambda R^{-1}\theta = 0, \tag{24}$$

$$(1 + R^{-1/2}\xi)\theta'' + R^{-1/2}\theta' + \sigma(\phi\theta' - \phi'\theta) = 0, \tag{25}$$

subject to the boundary conditions given in (5) and where primes now denote differentiation with respect to ξ. Equations (24, 25) suggest an expansion in powers of $R^{-1/2}$, the leading-order term just being the forced-convection limit discussed in [8].

For convection to have an effect at leading order we require λ to be large, specifically of $O(R)$. This leads us to put

$$\lambda = \mu R \quad \text{with } \mu \text{ of } O(1). \tag{26}$$

The problem for the leading-order terms $\phi_0,\ \theta_0$ is now

$$\phi_0''' + 1 + \phi_0\phi_0'' - \phi_0'^2 + \mu\theta_0 = 0, \tag{27}$$

$$\theta_0'' + \sigma(\phi_0\theta_0' - \phi_0'\theta_0) = 0, \tag{28}$$

still subject to the boundary conditions that

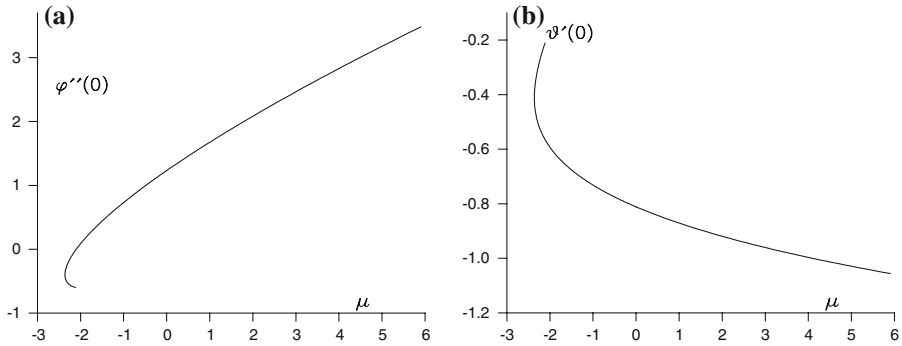

Fig. 5 Plots of (**a**) $\phi_0''(0)$ and (**b**) $\theta_0'(0)$ against $\mu = \lambda\, R^{-1}$ for the solution for large R given by (27–29) for $\sigma = 1$

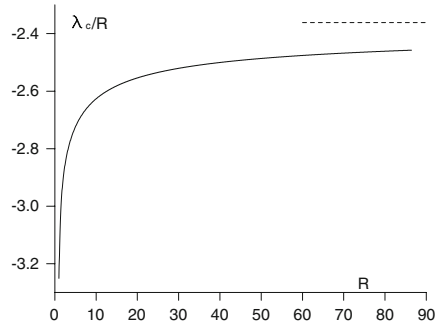

Fig. 6 A plot of $\lambda_c\, R^{-1}$ against R for $\sigma = 1$. The asymptotic limit (30) for R large is shown by the broken line

$$\phi_0(0) = 0,\ \phi_0'(0) = 0,\ \theta_0(0) = 1, \quad \phi_0' \to 1,\ \theta_0 \to 0 \quad \text{as}\ \ \xi \to \infty. \tag{29}$$

Equations (27–29) have to solved numerically and graphs of $\phi_0''(0)$ and $\theta_0'(0)$ for $\sigma = 1$ plotted against μ are shown in Fig. 5. From these figures we see that there is a critical value μ_c of μ with dual solutions for $0 > \mu > \mu_c$ and no solutions for $\mu < \mu_c$. For $\sigma = 1$, we find that $\mu_c = -2.3618$, giving

$$\lambda_c \sim -2.3618R + \cdots \quad \text{as}\ \ R \to \infty. \tag{30}$$

For $\mu > 0$ there is only one solution with both $\phi_0''(0)$ and $-\theta_0'(0)$ increasing as μ is increased.

Expression (30) shows a linear increase in $|\lambda_c|$ with R, as noted previously about Fig. 3, and to confirm this asymptotic behaviour we plot the values of $\lambda_c R^{-1}$ obtained from our numerical integrations to find λ_c against R in Fig. 6. The numerically determined values approach this asymptotic limit (shown by the broken line), though only slowly as R is increased, suggesting that the $O(R^{-1/2})$ correction has a significant effect even at moderately large values of R.

For μ large we can recover expressions (22) by putting

$$\phi_0 = \mu^{1/4}\,\overline{\phi}_0, \quad \overline{\xi} = \mu^{1/4}\,\xi. \tag{31}$$

When (31) is substituted in equations (27–29) and then $\mu \to \infty$, we obtain equations (15–17) and, on using (26), the leading-order terms in (22).

4.3 R small

The behaviour of the solution for R small depends on whether λ is small or of $O(1)$. We start with the latter case, assuming that $\lambda > 0$.

4.3.1 λ of O(1)

For this case we start in an inner region where η is of $O(1)$ and scale

$$f = A(R)\, g, \quad \theta = 1 + B(R)\, h. \tag{32}$$

The scaling factors A and B are to be determined, though we assume that

$$A(R) \gg 1, \quad B(R) \ll 1, \quad \frac{RA}{B} \ll 1, \quad AR \ll 1. \tag{33}$$

When (32) is substituted in (3, 4) and (33) is taken, the leading-order terms g_0, h_0 are given by, on satisfying the boundary condtions on $\eta = 1$,

$$g_0 = a_0(\eta \log \eta - \eta + 1), \quad h_0 = b_0 \log \eta \tag{34}$$

for constants a_0, b_0 to be determined. Before continuing the solution in the inner region, we next consider the outer region.

For the outer region we write

$$f = R^{-1}G, \quad \theta = \frac{\beta^2}{R} H, \quad Y = \beta\eta, \quad \text{where } \beta = \beta(R) \ll 1, \ \frac{R}{\beta} \ll 1 \tag{35}$$

with the scaling factor $\beta(R)$ also to be determined. When (35) is substituted in (3, 4) and the assumptions for β given in (35) applied, we find that the leading-order problem in the outer region is

$$YG''' + G'' + GG'' - G'^2 + \lambda H = 0, \quad YH'' + H' + \sigma(GH' - G'H) = 0, \tag{36}$$

subject to the outer boundary conditions at leading order that

$$G' \to 0, \quad H \to 0 \quad \text{as } Y \to \infty. \tag{37}$$

To find the inner boundary conditions for (36) we need to match with the inner region.

We can express the inner solution (34) as, on using (35),

$$\begin{aligned} f &\sim \tfrac{A(R)}{\beta}\, a_0 Y[\log Y + (-\log\beta) - 1] + \cdots, \\ \theta &\sim [1 + b_0 B(R)(-\log\beta)] + b_0 B(R) \log Y + \cdots. \end{aligned} \tag{38}$$

From (38) we choose

$$A(R) = \frac{\beta}{R(-\log\beta)}, \quad B(R) = \frac{1}{(-\log\beta)} = \frac{\beta^2}{R}, \quad b_0 = -1. \tag{39}$$

Hence $\beta(R)$ is given implicitly by

$$\beta^2(-\log\beta) = R, \quad \text{with } \beta \sim \frac{\sqrt{2}\, R^{1/2}}{(-\log R)^{1/2}} + \cdots \quad \text{as } R \to 0. \tag{40}$$

We note that (39, 40) are consistent with the assumptions in (33) and (35). Expressions (38) then give, at leading order,

$$G \sim a_0 Y + \cdots, \quad H \sim -\log Y + \cdots \quad \text{as } Y \to 0. \tag{41}$$

To get higher order terms in (41) we need to consider the inner region again. On using (39) we see that an expansion of the form

$$g = g_0 + \frac{g_1}{(-\log\beta)} + \cdots + O(\beta), \quad h = h_0 + \frac{h_1}{(-\log\beta)} + \cdots + O(\beta) \tag{42}$$

is required, where the $O(\beta)$ terms in (42) also include terms in

$$\beta(-\log\beta)^2, \quad \beta(-\log\beta), \quad \beta(-\log\beta)^{-1}$$

and $h_1 = b_1 \log \eta$ for some constant b_1. When (42) is substituted in (3, 4) and using (32, 35) we find, after some calculation, that the inner boundary condition (41) for the outer region becomes modified to

$$G \sim a_0 Y + \frac{\lambda}{2} Y^2 \log Y + \frac{1}{2}\left(a_0^2 - \frac{5\lambda}{2} - \lambda b_1\right) Y^2 + \cdots,$$
$$H \sim -\log Y + b_1 - \sigma a_0 Y \log Y + \sigma a_0 (b_1 + 2) Y + \cdots \quad \text{as } Y \to 0. \tag{43}$$

We can remove the parameter λ from this problem by writing $\overline{Y} = \lambda^{1/2} Y$ and then the problem in the outer region becomes

$$\overline{Y} G''' + G'' + G G'' - G'^2 + H = 0, \quad \overline{Y} H'' + H' + \sigma (G H' - G' H) = 0, \tag{44}$$

subject to the conditions that

$$G' \to 0, \quad H \to 0 \quad \text{as } \overline{Y} \to \infty \tag{45}$$

and

$$G \sim \overline{a}_0 \overline{Y} + \frac{\overline{Y}^2}{2} \log \overline{Y} + \frac{1}{2}\left(\overline{a}_0^2 - \frac{5}{2} - \overline{b}_1\right) \overline{Y}^2 + \cdots,$$
$$H \sim -\log \overline{Y} + \overline{b}_1 - \sigma \overline{a}_0 \overline{Y} \log \overline{Y} + \sigma \overline{a}_0 (\overline{b}_1 + 2) \overline{Y} + \cdots \quad \text{as } \overline{Y} \to 0, \tag{46}$$

where $\overline{a}_0 = \lambda^{-1/2} a_0$ and $\overline{b}_1 = b_1 + \frac{1}{2} \log \lambda$.

The problem given by (44–46) has to be solved numerically to determine the constants $\overline{a}_0$ and $\overline{b}_1$ and we find, for $\sigma = 1$, that $\overline{a}_0 = 1.0016$, $\overline{b}_1 = -1.2396$. This then gives for small R and $\sigma = 1$,

$$\left(\frac{\mathrm{d}^2 f}{\mathrm{d}\eta^2}\right)_{\eta=1} = \frac{1}{\beta(-\log\beta)^2}(1.0016\lambda^{1/2} + \cdots),$$
$$\left(\frac{\mathrm{d}\theta}{\mathrm{d}\eta}\right)_{\eta=1} = -\frac{1}{(-\log\beta)}\left(1 + \frac{1.2396 + \frac{1}{2}\log\lambda}{(-\log\beta)} + \cdots\right), \tag{47}$$

with β given in terms of R by (40). Equations (3, 4) were solved numerically with $\lambda = 1$ for small values of R. The solution domain increases as R is decreased, in line with (35), and the outer boundary condition had to be applied at increasingly larger values of $\eta = \eta_\infty$ as R was decreased, the results shown in Fig. 7 were obtained using $\eta_\infty = 250$. In Fig. 7 we give plots of $f''(1)$ and $\theta'(1)$ against R obtained from our numerical integrations, the values obtained from (47) are shown by broken lines. The agreement with the asymptotic forms for small R is not particularly good, though both solutions are following the same trend. This difference can, perhaps, be explained by the fact that the approach to the asymptotic forms (47) is only very slow, with correction terms of $(-\log\beta)^{-1} \sim (-\log R)^{-1}$ and hence R has to be extremely small for these correction terms to have only a small effect. In practice we probably require values of R too small for obtaining reasonably accurate numerical solutions. At these very small values of R, η_∞ needs to be extremely large leading to errors in the shooting method employed to solve the two-point boundary-value problem.

4.3.2 λ small

We can see, particularly from (36, 37), that, when λ is of $O(1)$, the flow is driven at leading order only by the natural-convection effects. The forced flow enters the solution at higher order. However, when λ is small, this cannot be the case and to get an estimate on λ when the forced-convection effects have an influence at leading order, we see from (35) that the buoyancy term included in equation (36) is of $O(\lambda\beta^2 R^{-1})$ whereas the forced-convection term is of $O(R)$. This suggests, on using (40), that these two effects will be comparable when $\lambda \sim R(-\log R)$ and leads us to put

$$\lambda = R(-\log R)\,\nu \quad \text{with } \nu \text{ of } O(1) \text{ for } R \text{ small}. \tag{48}$$

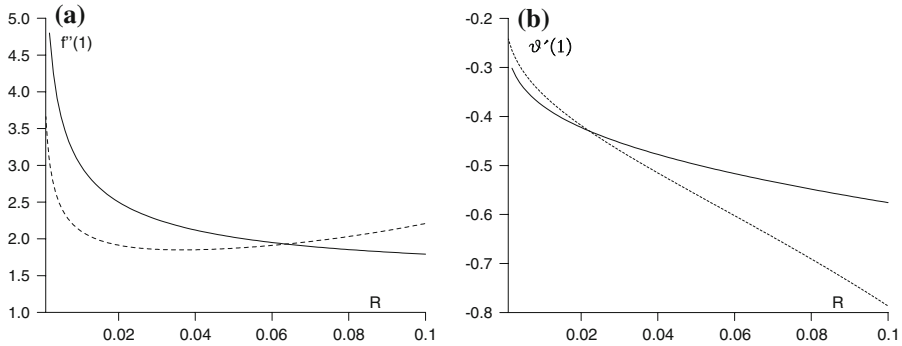

Fig. 7 Plots of (**a**) $f''(1)$ and (**b**) $\theta'(1)$ against R for $\lambda = 1$, $\sigma = 1$ for small R obtained from the numerical solution of Eqs. (3, 4) subject to boundary conditions (5). The asymptotic expressions (47) are shown by the broken lines

We start our solution for this case in the inner region where we have at leading order, motivated by our previous solution for λ of $O(1)$,

$$f \sim \frac{1}{(-\log R)}\, c_0(\eta \log \eta - \eta + 1) + \cdots, \quad \theta \sim 1 + \frac{1}{(-\log R)}\left(-\log \eta + \frac{d_1}{(-\log R)} \log \eta + \cdots\right) \tag{49}$$

for constants c_0 and d_1 to be determined. For the outer region we now put

$$f = \frac{1}{R}\, G, \quad \theta = \frac{1}{(-\log R)}\, H, \quad Y = R\,\eta. \tag{50}$$

Applying (50) in (3, 4) gives, at leading order,

$$YG''' + G'' + 1 + GG'' - G'^2 + \nu H = 0, \quad YH'' + H' + \sigma(GH' - G'H) = 0, \tag{51}$$

now subject to the outer boundary conditions

$$G' \to 1, \quad H \to 0 \quad \text{as} \quad Y \to \infty \tag{52}$$

and, on matching with the inner region,

$$G \sim c_0 Y + \cdots, \quad H \sim -\log Y + d_1 + \cdots \quad \text{as} \quad Y \to 0. \tag{53}$$

We note that ν cannot be scaled out of problem (51–53) (as it could previously) and that, for $\nu = 0$ (forced-convection limit)

$$c_0 = 1, \quad G = Y, \quad H = -\frac{\mathrm{e}^{-\sigma Y}\log(\sigma Y)}{(1+\sigma Y)} + (1+\sigma Y)\int_{\sigma Y}^{\infty} \frac{\mathrm{e}^{-v}(3+v)\log v}{(1+v)^3}\,\mathrm{d}v, \tag{54}$$

giving

$$d_1 = \int_0^{\infty} \frac{\mathrm{e}^{-v}(3+v)\log v}{(1+v)^3}\,\mathrm{d}v - \log\sigma = -1.4448 - \log\sigma.$$

Plots of c_0 against ν obtained by solving (51–53) numerically are given in Fig. 8. This figure shows that there is a critical value ν_c of ν, with $\nu_c = -0.9832$ for $\sigma = 1$, and dual solutions for $0 > \nu > \nu_c$. This gives

$$\lambda_c \sim -0.9832R(-\log R) + \cdots \quad \text{as} \quad R \to 0. \tag{55}$$

For $\nu > 0$ there is only one solution and the problem given by (44–46) can be recovered for ν large by putting $\overline{Y} = \nu^{1/2}Y$ in (51–53) and letting $\nu \to \infty$.

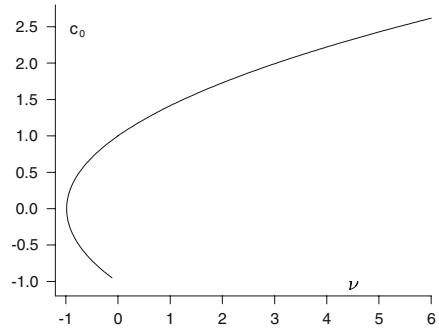

Fig. 8 A plot of c_0 against ν, defined in (48), for $\sigma = 1$ arising in the small R, small λ problem (51–53)

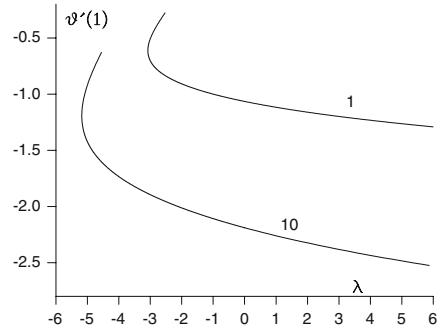

Fig. 9 Plots of $\theta'(1)$ against λ for $R = 1$ and $\sigma = 1,\ 10$ obtained from the numerical solution of Eqs. (3, 4) subject to boundary conditions (5)

5 Solution for σ large

Our previous numerical results were for the case $\sigma = 1$ and we expect qualitatively similar behaviour when σ is of $O(1)$, typical of gases. For liquids (water) σ is somewhat larger and it is thus worth briefly considering the large σ limit. Following the treatment in [20,21] we expect that, for σ large, the solution to involve a relatively thin thermal inner layer and a thicker outer viscous flow region. In the inner region we have

$$\eta = 1 + \sigma^{-1/3}\tau, \quad f = \sigma^{-2/3}\Phi \tag{56}$$

with θ left unscaled. At leading order, for σ large, we obtain

$$\Phi''' = 0, \quad \theta'' + R(\Phi\theta' - \Phi'\theta) = 0, \tag{57}$$

subject to

$$\Phi(0) = 0,\ \Phi'(0) = 0, \quad \theta(0) = 1,\ \theta \to 0 \ \text{ as } \ \tau \to \infty, \tag{58}$$

with the outer condition on Φ relaxed at this stage and where primes denote differentiation with respect to τ.

Equations (57, 58) give

$$\Phi = A_0\tau^2 \tag{59}$$

for some constant $A_0 = A_0(R)$ to be determined and

$$\theta = \frac{\left(\frac{2}{3}\right)!}{3\left(\frac{1}{3}\right)!}\,\mathrm{e}^{-s}\,U\left(\frac{4}{3};\frac{2}{3};s\right) \quad \text{where } \ s = \frac{1}{3}\,(RA_0)\tau^3 \tag{60}$$

in terms of confluent hypergeometric functions [22]. Expressions (56) and (60) give

$$\left(\frac{\mathrm{d}\theta}{\mathrm{d}\eta}\right)_{\eta=1} = -\sigma^{1/3}(RA_0)^{1/3}\,\frac{3^{2/3}\left(\frac{2}{3}\right)!^2}{2\left(\frac{1}{3}\right)!^2} + \cdots \quad \text{as } \ \sigma \to \infty. \tag{61}$$

Expression (61) shows that the heat transfer increases as σ is increased, being of $O(\sigma^{1/3})$ for σ large.

To determine the constant A_0 we need to consider the outer region, in which we can neglect the temperature and write $\eta = 1 + \overline{\eta}$. This leads to

$$(1 + \overline{\eta})f''' + f'' + R(1 + ff'' - f'^2) = 0 \tag{62}$$

and, on matching with the inner region, that

$$f \sim A_0\overline{\eta}^2 + \cdots \quad \text{as } \ \overline{\eta} \to 0, \quad f' \to 0 \quad \text{as } \ \overline{\eta} \to \infty. \tag{63}$$

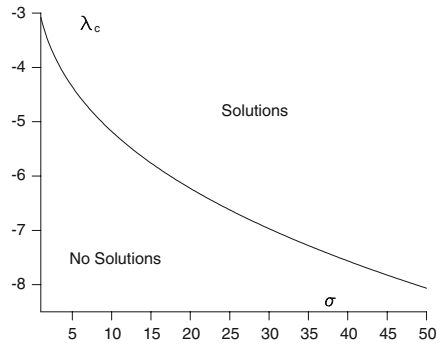

Fig. 10 A plot of the critical value λ_c of λ against σ for $R = 1$. The region in the (λ, σ) parameter plane where solutions exist is labelled on the figure

Equations (62, 63) are essentially the forced-convection limit with the solution given by [8]. Their solution then gives A_0 in terms of R. For R large [8] show that $A_0 \sim 0.6163\, R^{1/2} + \cdots$, giving $\left(\frac{\mathrm{d}\theta}{\mathrm{d}\eta}\right)_{\eta=1}$ of $O(R^{1/2}\sigma^{1/3})$ for R and σ large.

The leading-order problem (57, 58, 62, 63) for σ large does not give a critical value for λ. In fact, the solution is independent of λ at leading order, with the buoyancy forces arising at $O(\sigma^{-1/3})$ in the inner region. This suggests that the critical value λ_c will, for a given value of R, decrease to large negative values as σ is increased. We illustrate this in Fig. 9 with a plot of $\theta'(1)$ against λ for $R = 1$ and $\sigma = 10$ to compare with the results for $\sigma = 1$. This figure clearly shows that the critical values λ_c has decreased for $\sigma = 10$ over that for $\sigma = 1$, giving a greater range of λ for solutions in the opposing case. The values of $\theta'(1)$ have, for a given λ, also decreased for $\sigma = 10$, in line with expression (61). In Fig. 10 we plot λ_c against σ again for $R = 1$, showing that λ_c decreases relatively slowly as σ is increased, as can be expected from the above analysis for the large λ case.

6 Conclusions

We have considered the mixed convection boundary-layer flow around an axisymmetric stagnation point. The equations for the flow and temperature fields reduce to similarity form (3–5) and involve the three parameters, the Prandtl number σ, a Reynolds number R and a mixed convection parameter λ, as defined in (6). The similarity equations were solved numerically for representative values of the parameters R and λ; see Figs. 1 and 2. The main conclusions from these numerical integrations were that, for $\lambda < 0$ (opposing flow), there was a critical value λ_c of λ at which there was a saddle-node bifurcation with dual solutions for $\lambda_c < \lambda < 0$ and no solutions for $\lambda < \lambda_c$. For $\lambda \geq 0$ (aiding flow) there was a single solution for all λ. An asymptotic solution for λ large was derived, with the results summarized in (22).

The occurrence of dual solutions for opposing flows is not unexpected and is consistent with many previous studies of similarity solutions in mixed convection, see [18,19,23] for example. The critical value λ_c was seen to depend on R (and on σ), see Fig. 3. The possibilities of solutions having only a limited range of existence and the existence of dual solutions for opposing flows was not noticed by Gorla [12]. The reason for this is that the results in [12] were all for $R = 100$ and our study suggests that the value of λ_c for this value of R is quite large, well beyond the values for the mixed convection parameter taken in [12]. A solution for R large was obtained which showed that λ_c is of $O(R)$ in this case, as given in (30) for $\sigma = 1$. Thus for strong external flows (large R) boundary-layer flows are still possible even when there are strongly opposing buoyancy forces. For R small the flow was seen to be driven predominantly by the buoyancy forces when λ is of $O(1)$, as summarized in (47). However, for λ small both buoyancy and the external flow have comparable effects, giving a critical value of $O(R(-\log R))$ for R small, as given by (55) for $\sigma = 1$. The effect of weak external flows is then to severely limit the range of λ where there can be opposing flows.

The effect of having large values for the Prandtl number σ is to confine the thermal effects to a thin layer, of thickness $O(\sigma^{-1/3})$, next to the cylinder with the outer flow being essentially given by forced convection. A consequence of this is, for opposing flows, to decrease λ_c to large negative values, with solutions then being possible for a large range of the mixed convection parameter.

Acknowledgements CR was supported by the CEEX grant No 2-CEx06-11-96/2006. JM and IP were both supported by a Royal Society (London) Joint Project Grant.

References

1. Hiemenz K (1911) Die Grenzschicht an einem in den gleich formigen Flussigkeitsstrom eingetacuhten geraden Kreisszylinder. Dinglers Polytech J 326:321–324
2. Eckert ERG (1942) Die Berechnung des Wärmeüberganges in der laminaren Grenzschicht um stromter Korper. VDI – Forchungsheft 416:1–24
3. Gorla RSR (1976) Heat transfer in an axisymmetric stagnation flow on a cylinder. Appl Sci Res 32:541–553
4. Hommann F (1936) Der Einfluss grosser Zähigkeit bei der Stromung um den Cylinder und um die Kugel. J Appl Math Phys (ZAMP) 16:153–164
5. Smith FT (1974) Three dimensional stagnation point flow in a corner. Proc R Soc Lond A 344:489–507
6. Wang CY (1974) Axisymmetric stagnation flow on a cylinder. Quart Appl Math 32:207–213
7. Gorla RSR (1978) Nonsimilar axisymetric stagnation flow on a moving cylinder. Int J Eng Sci 16:392–400
8. Weidman PD, Putkaradze V (2003) Axisymmetric stagnation flow obliquely impinging on a circular cylinder. Eur J Mech B/Fluids 22:123–131
9. Weidman PD, Mahalingam S (1997) Axisymmetric stagnation-point flow impinging on a transversely oscillating plate with suction. J Eng Math 31:305–318
10. Gorla RSR (1979) Unsteady viscous flow in the vicinity of an axisymmetric stagnation point on a circular cylinder. Int J Eng Sci 17:87–93
11. Ramachandran N, Chen TS, Armaly BF (1988) Mixed convection in stagnation flows adjacent to vertical surface. J Heat Trans 110:173–177
12. Gorla RSR (1993) Mixed convection in an axisymmetric stagnation flow on a vertical cylinder. Acta Mech 99:113–123
13. Kuiken HK (1974) The thick free-convective boundary-layer along a semi-infinite isothermal vertical cylinder. J Appl Math Phys (ZAMP) 25:497–514
14. Naraian IP, Uberoi MS (1972) Combined forced and free convection heat transfer from thin needles in a uniform stream. Phys Fluids 15:1879–1882
15. Naraian IP, Uberoi MS (1973) Combined forced and free convection over thin needles. Int J Heat Mass Trans 16:1505–1511
16. Chen ILS (1987) Mixed convection flow about slender bodies of revolution. J Heat Trans 109:1033–1036
17. Wang CY (1990) Mixed convection on a vertical needle with heated tip. Phys Fluids A 2:622–625
18. Merkin JH (1985) On dual solutions occurring in mixed convection in a porous medium. J Eng Math 20:171–179
19. Merkin JH, Mahmood T (1989) Mixed convection boundary layer similarity solutions: prescribed wall heat flux. J Appl Math Phys (ZAMP) 40:51–68
20. Stewartson K, Jones LT (1957) The heated vertical plate at high Prandtl number. J Aeronaut Sci 24:379–380
21. Kuiken HK (1968) The heated vertical plate at high Prandtl number free convection. J Eng Math 2:355–371
22. Slater LJ (1960) Confluent hypergeometric functions. Cambridge University Press, Cambridge
23. Wilks G, Bramley JS (1981) Dual solutions in mixed convection. Proc R Soc Edinb 87A:349–358